Int. J. Nano Dimens., 15 (1): 93-101, Winter 2024

ORIGINAL ARTICLE

Quantum spin hall effect on pseudo-graphene zigzag nanoribbons

Javad Ghorbani[1], Mehdi Ghaffarian[*2], Hasan Tashakori[1], Alireza Baradaran[2]*

[1] Department of Physics, Qom Branch, Islamic Azad University, Qom, Iran
[2]Department of Physics, University of Qom, Qom, Iran

Received 30 November 2023, revised 06 January 2024, accepted 11 January 2024, available online 15 January 2024

Abstract
This research explores how two-dimensional honeycomb materials can be used in advanced electronics, focusing on zigzag honeycomb nanoribbons. These nanoribbons can create zero-energy band gaps, enabling helical spin current edge states. The study investigates the quantum spin Hall state, showcasing the adaptability of the Kane-Mele model in various honeycomb lattices. In addition to the theoretical discussions, this study presents a detailed Hamiltonian, performs band structure computations, and introduces a novel spin-filtering technique for zigzag nanoribbons. This method enhances our understanding of edge-localized quantum states and can revolutionize spintronics. By revealing the quantum states in honeycomb nanoribbons, this study contributes to the advancement of electronics and offers a promising path for highly efficient spin-based technologies.

Keywords: *Haldane Model; Kane-Mele Model; Pseudo-Graphene; Quantum Spin Hall Effect; Topological Insulator; Two-Dimensional Honeycomb Materials; Zigzag Nanoribbon.*

How to cite this article
Ghorbani J., Ghaffarian M., Tashakori H., Baradaran A., Quantum spin hall effect on pseudo-graphene zigzag nanoribbons. Int. J. Nano Dimens., 2024; 15(1): 93-101.

INTRODUCTION

Interest in two-dimensional honeycomb crystalline materials has surged due to their potential in advanced electronics with enhanced processing capabilities [1-3]. These materials are particularly appealing because of their edge structures, with zigzag edges playing a crucial role in defining the nanoscale electrical characteristics [4, 5]. The edge states in honeycomb zigzag nanoribbons (ZNRs) are significant because they form restricted edge channels concentrated at the edges of the bulk. In contrast to armchair edges, zigzag edges create zero-energy band gaps, allowing edge carriers to propagate freely through their channels [6-8]. The exponential decay of zigzag edge states away from the edges is noteworthy and aids in understanding the transport phenomena, which is crucial for developing highly efficient electrical nanodevices [9, 10].

Silicene and germanene, materials with intrinsic spin-orbit interaction (SOI), hold promise for discovering quantum spin Hall (QSH) states. Graphene-like materials undergo a captivating transition to the QSH phase when the SOI is enhanced, affecting the spin degree of freedom. Kane and Mele first predicted this phenomenon [11, 12] by developing band structures of graphene zigzag nanoribbons (ZNRs) with SOI components using the Haldane model [13]. This revealed gap formation around the Fermi energy, where time-reversal symmetry protects two spin-filtered channels, resulting in edge states with rotational motion and topological insulator properties [14]. Kane-Mele's model extends beyond graphene to various honeycomb lattices like silicene, germanene [15, 16], stanene [17], and more [18, 19], showcasing their potential for spintronics applications [20-21]. Some researchers have worked on surrounding issues [22-24]. Certainly, by applying DFT and incorporating electron-electron interactions, as done in other studies, the calculations can be extended and enhanced. This approach allows for a more comprehensive exploration of the system, taking into account the

* Corresponding Author Email: *m.ghaffarian@yahoo.com*

electron-electron interactions for a more accurate representation [25-28].

This paper is organized into several sections for a comprehensive examination of our study. Section 2 introduces the Hamiltonian under Spin-Orbit Interaction (SOI), forming the basis for understanding the electronic states in honeycomb structures. Using this Hamiltonian, we explore the band structure of a honeycomb sheet, revealing the intricate influence of the SOI and the resulting band gap.

Section 3, at the core of our findings, is divided into two key subsections. The first study examines the impact of the SOI on the bulk band spectrum, uncovering quantum dynamics. Simultaneously, we investigate the size-dependent band gap in Zigzag Nanoribbons (ZNRs), which is crucial for nanoscale device design. In the second subsection, we pioneer the exploration of ZNRs under varying SOI strengths by introducing a groundbreaking spin-filtering technique with significant potential for spintronics.

Finally, section 4 concludes the study with a concise summary of the results and their implications. This conclusion highlights the broader significance of our findings and provides direction for future research in the dynamic fields of spintronics and quantum materials.

MATERIALS AND METHODS

The Hamiltonian for the honeycomb lattice with two unique bases, as illustrated in Fig. 1(a), is as follows, disregarding the SOI,

$$\mathrm{H} = \sum_{\mathrm{i}} \varepsilon_{\mathrm{a}} \mathrm{c}_{\mathrm{i}}^{\dagger} \mathrm{c}_{\mathrm{i}} + \sum_{\mathrm{i}} \varepsilon_{\mathrm{b}} \mathrm{b}_{\mathrm{i}}^{\dagger} \mathrm{b}_{\mathrm{i}} + \mathrm{t} \sum_{\langle \mathrm{i,j} \rangle} \left(\mathrm{c}_{\mathrm{i}}^{\dagger} \mathrm{b}_{\mathrm{j}} \mathrm{b}_{\mathrm{j}}^{\dagger} \mathrm{c}_{\mathrm{i}} \right). \quad (1)$$

To expand this framework based on Haldane's model and account for the SOI, we need to incorporate the Hamiltonian of the SOI into Equation (1). The general form of the SOI Hamiltonian is

$$\mathrm{H} = \frac{\hbar \mathrm{e}}{4\mathrm{m}_0^2 \mathrm{c}^2} \left(\vec{\nabla} \mathrm{V} \times \vec{\mathrm{P}} \right). \vec{\sigma} = -\frac{\hbar \mathrm{e}}{4\mathrm{m}_0^2 \mathrm{c}^2} \left(\vec{\mathrm{E}} \times \vec{\mathrm{P}} \right). \vec{\sigma}, \quad (2)$$

here $\hbar$, m_0, e and c are Planck's constant, electron mass, electron charge, and the speed of light, respectively. The crystal lattice ions create an electric potential $V(\vec{E})$ due to the coplanar direction of the electric field within the plane. $\vec{\mathrm{P}}$ signifies the magnitude and direction of electron movement, influenced by electron hopping from one position to another. Fig. 1(b) illustrates the electric-field direction of the graphene honeycomb network. The presence of mirror symmetry results in a zero total electric field at the hopping location, preventing the spin-orbit effect in electron hopping between adjacent sites. However, due to the absence of symmetry, a non-zero electric field emerges, leading to a non-zero SOI.

By setting $\vec{P} = i\alpha \vec{d}_{ij}$ (where $\vec{d}_{ij}$ is the hopping vector to the second neighbors and between atomic positions i and j), the spin-orbit Hamiltonian can be rewritten as follows,

$$H_{so} = i \frac{\hbar e \alpha}{4 m_0^2 c^2} \left(\vec{E} \times \vec{d}_{ij} \right). \vec{\sigma}. \quad (3)$$

Because $\vec{E}, \vec{d}_{ij}$ are both on the $(x-y)$ plane, their cross product is in the z-direction, hence H_{so} is as follows,

$$H_{so} = i \frac{\hbar e \alpha \left| \vec{E} \times \vec{d}_{ij} \right|}{4 m_0^2 c^2} \nu_{ij} \sigma_z = i t_{so} \nu_{ij} \sigma_z, \quad (4)$$

where $\nu_{ij} = \frac{\vec{d}_i \times \vec{d}_j}{|\vec{d}_i \times \vec{d}_j|}$ and t_{so} is the intensity of the SOI. The electron experiences varying electric fields when hopping to the second neighbor due to the different basic atoms in the honeycomb lattice. According to Fig. 1(b), when hopping to the second neighbor in the type A atom, there is a field E, and when hopping to the second neighbor in the type B atom, there is a field E'; hence, the value of t_{so} for these states and the Hamiltonian of SOI will be different. It will look like this,

$$H_{so} = i t_{so} \sum_{\langle i,j \rangle} \nu_{ij} c_i^{\dagger} \sigma_z c_j + i t'_{so} \sum_{\langle i,j \rangle} \nu_{ij} b_i^{\dagger} \sigma_z b_j. \quad (5)$$

Finally, by incorporating the SOI, the overall Hamiltonian for the honeycomb lattice is stated as follows,

$$\begin{aligned} H = \sum_i \varepsilon_a c_i^{\dagger} c_i + \sum_i \varepsilon_b b_i^{\dagger} b_i + t \sum_{\langle i,j \rangle} \left(c_i^{\dagger} b_j b_j^{\dagger} c_i \right) \\ + i t_{so} \sum_{\langle i,j \rangle} \nu_{ij} c_i^{\dagger} \sigma_z c_j \\ + i t'_{so} \sum_{\langle i,j \rangle} \nu_{ij} b_i^{\dagger} \sigma_z b_j. \end{aligned} \quad (6)$$

In this relation, t'_{so}, t_{so} represent the SOI for atoms of type B and A, σ_z represents the Pauli matrix, $b_i^{\dagger}, c_i^{\dagger}$ are creation operators and b_i, c_i are annihilation operators for π electrons in the *i*-th

site with σ spin, $\langle i,j\rangle$ indicates the sum over the first neighbor, and $\langle\langle i,j\rangle\rangle$ indicates the sum over the second neighbor.

The Hamiltonian for a two-dimensional pseudo-graphene lattice takes the shape of a 4x4 matrix and has the following formula,

$$H(k_x,k_y)=\begin{pmatrix}H(k) & 0\\ 0 & H^*(-k)\end{pmatrix}, \quad 7$$

where $H(k)$ is a 2x2 Hamiltonian for spin-up levels and $H^*(-k)$, representing the time-reversal of $H(-k)$, is for spin-down levels.

In the next steps, we compute the energy bands for spin-up levels, and subsequently, utilizing the time-reversal symmetry, we derive the energy bands for spin-down levels.

Hamiltonian $H(k)$ has the following general form,

$$H_{\uparrow}(k)=\begin{pmatrix}\varepsilon_a+2t_{so}h(k_x,k_y) & |c|\\ |c|^* & \varepsilon_b-2t'_{so}h(k_x,k_y)\end{pmatrix}, \quad 8$$

the value of $h(k_x,k_y)$ in this expression is

$$h(k_x,k_y)=\left(-sin(k_xa)+sin\left(\frac{k_x}{2}a+\frac{\sqrt{3}}{2}k_ya\right)-sin\left(\frac{-k_x}{2}a+\frac{\sqrt{3}}{2}k_ya\right)\right). \quad 9$$

The value of c in this context is

$$|c|=\sqrt{3+2\left(cos\left(\frac{k_x}{2}a+\frac{\sqrt{3}}{2}\frac{k_y}{2}a\right)+cos\left(\frac{-k_x}{2}a+\frac{\sqrt{3}}{2}\frac{k_y}{2}a\right)+cos(k_xa)\right)}. \quad 10$$

By diagonalizing the Hamiltonian in equation (8),

$$\varepsilon_{\uparrow\pm}=(t_{so}-t'_{so})H(k_x,k_y)\pm\sqrt{\left(\frac{\Delta}{2}+(t_{so}+t'_{so})h(k_x,k_y)\right)^2+|c|^2}. \quad 11$$

Considering zero energy between the on-site energies, we obtain: $\varepsilon_b=-\frac{\Delta}{2},\varepsilon_a=\frac{\Delta}{2}$ where: $\varepsilon_b=-\frac{\Delta}{2},\varepsilon_a=\frac{\Delta}{2}$. Also, by using the time-reversal symmetry, we can obtain the spin-down energy bands as follows,

$$\varepsilon_{\downarrow\pm}=-(t_{so}-t'_{so})H(k_x,k_y)\pm\sqrt{\left(\frac{\Delta}{2}-(t_{so}+t'_{so})h(k_x,k_y)\right)^2+|c|^2}. \quad 12$$

The extrema of the valence and conduction bands in pseudo-graphene structures are positioned on the boundary of the first Brillouin zone at the positions $K=(\frac{4\pi}{3a},0),K'=(\frac{2\pi}{3a},\frac{2\pi}{\sqrt{3}a})$. The energy gap of spin-up and spin-down can be calculated by putting the coordinates of the K point in the relation (11) and (12).

$$\varepsilon_{g\uparrow}=\varepsilon_{+\uparrow}-\varepsilon_{-\uparrow}=\left|\Delta+\frac{3\sqrt{3}}{2}(t_{so}+t'_{so})\right|,\quad \varepsilon_{g\downarrow}=\varepsilon_{+\downarrow}-\varepsilon_{-\downarrow}=\left|\Delta-\tfrac{3\sqrt{3}}{2}(t_{so}+t'_{so})\right|. \quad 13$$

Additionally, at the K' point, the spin-up and spin-down energy gaps are as follows,

$$\varepsilon_{g\downarrow}=\varepsilon_{+\downarrow}-\varepsilon_{-\downarrow}=\left|\Delta+\frac{3\sqrt{3}}{2}(t_{so}+t'_{so})\right|,\quad \varepsilon_{g\uparrow}=\varepsilon_{+\uparrow}-\varepsilon_{-\uparrow}=\left|\Delta-\tfrac{3\sqrt{3}}{2}(t_{so}+t'_{so})\right|. \quad 14$$

If we consider the Fermi energy within the band gap, then: $\varepsilon_f=\varepsilon_-+\frac{\Delta}{2}=\frac{3\sqrt{3}}{2}(t_{so}-t'_{so})$.

RESULTS AND DISCUSSIONS

Effect of equal SOI for two bases in a unit cell on honeycomb pseudo-graphene and ZNR

Fig. 2 displays the energy band structures of a pseudo-graphene sheet with varying on-site energies for type A and type B atoms ε_A=0.5,ε_B=-0.5. The SOI of A type atoms, t_{so}, is considered equal to the SOI of B type atoms, t'_{so}. The paths used are illustrated in Fig. 1(c), following used *Γ-K-M-K'-Γ*.

Fig. 2(a) illustrates that when t_{so}=0, the energy bands of spin-up and spin-down overlap, leaving a gap equal to the energy difference on the sites of type A and type B atoms. With the introduction of SOI, the Hamiltonian establishes time-reversal symmetry, resulting in the split of spin-up and spin-down energy bands. This leads to an asymmetry between the spin-up and spin-down bands along the specified route. The spin-up energy band gap decreases at K' and increases at K, while the spin-down energy band gap increases at K' and decreases at K as depicted in Fig. 2(b). At a critical value $t_{so-c}=\frac{\Delta}{6\sqrt{3}}=0.096$ the band gap completely closes at the K' point for spin-up bands and at the K point for spin-down bands, as demonstrated in Fig. 2(c). When $t_{so}>t_{so\text{-}c}$, the energy band reopens, the valence states are replaced by conduction states, the energy band inverts, and the network enters the QSH state, as depicted in Fig. 2(d).

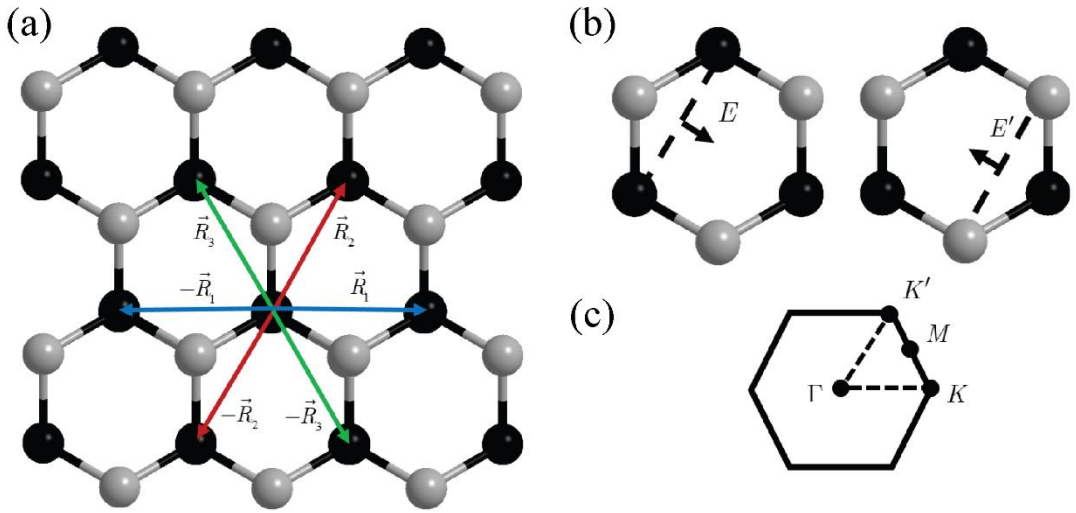

Fig. 1. a) Honeycomb pseudo-graphene lattice (with different bases), b) Electric field direction for honeycomb network, and c) high symmetry points in reciprocal lattice.

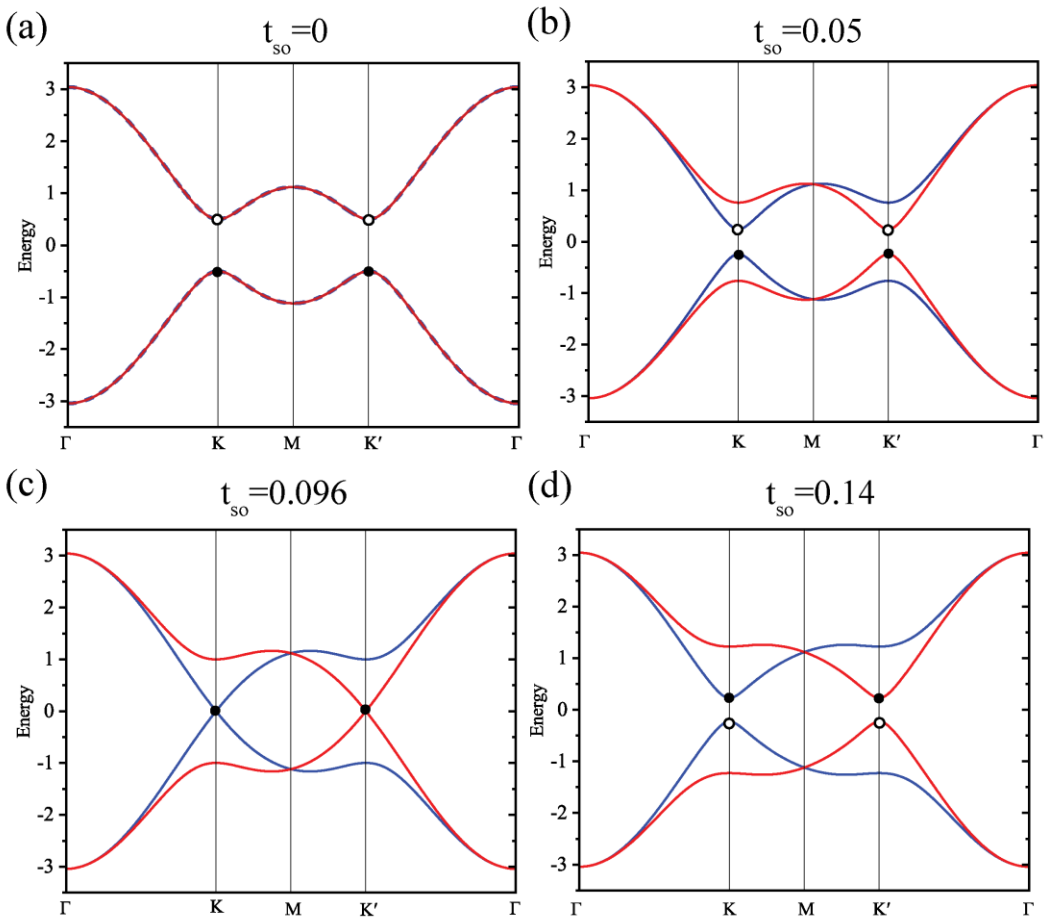

Fig. 2. a) The SOI is zero (t_{so}=0), b) by increasing the SOI of each lattice atom (t_{so}=0.05), it shows different behaviors for spin-up (blue) and spin-down (red) bands, c) until at a critical value ($t_{so\text{-}c}$=0.096), both closed, and d) it enters the QSH phase (t_{so}>$t_{so\text{-}c}$).

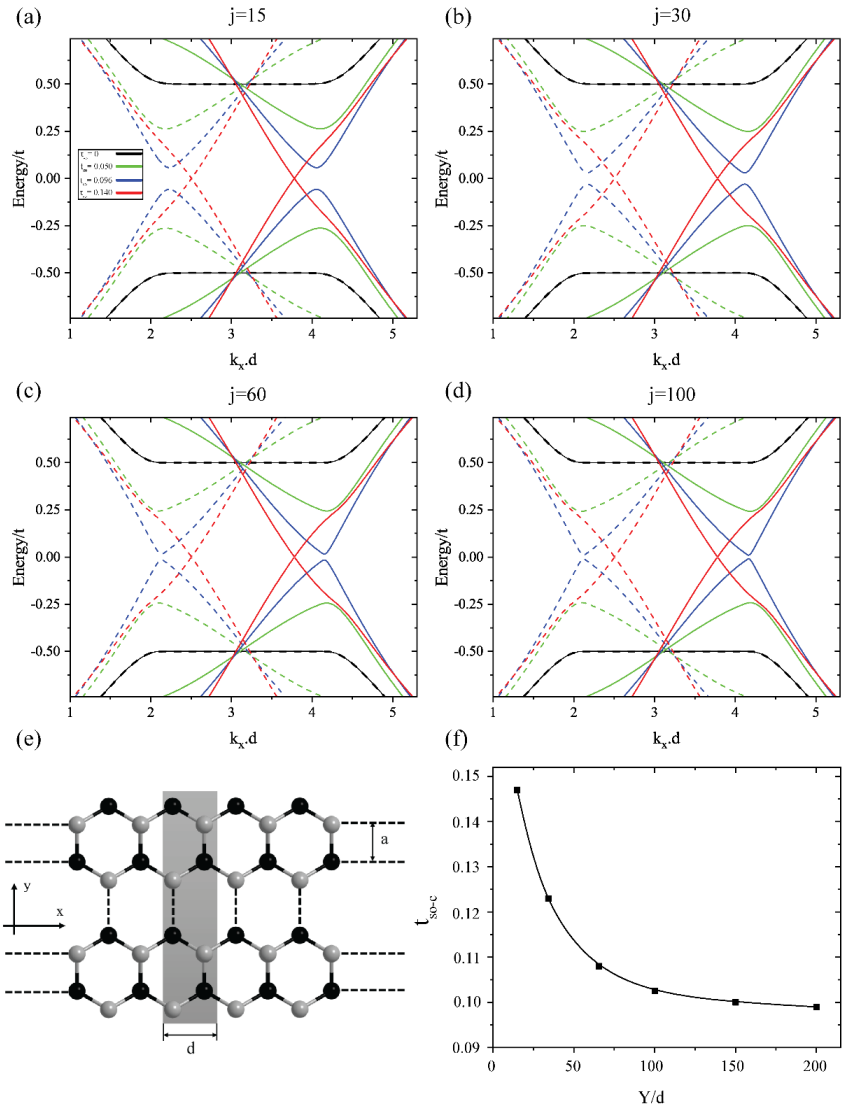

Fig. 3. a-d) With the increase in the size of the unit cell in the ZNR and the strength of the SOI, the gap closes and enters the QSH phase, spin-up band and spin-down depicted in continues and dashed lines, respectively, e) Honeycomb zigzag nanoribbon (ZNR) which is infinite in the x-direction and finite in the y-direction, f) Critical SOI as a function of the width of ZNR $Y=2|y|$ where the ribbon is considered from -y to y.

To investigate the impact of size on the transition to the QSH phase, we calculate the energy bands of zigzag pseudo-graphene nanoribbons with varying widths and bases. Fig. 3(a-d) illustrates the energy bands at the Fermi level for nanoribbons with widths of 15, 30, 60, and 100 nanometers, respectively. Each graph represents different spin-orbit intensities (t_{so} = 0, 0.05, 0.096, 0.14) for a specific nanoribbon width. The structure of the ZNRs, which is infinite in the x-direction and finite in the y-direction, is shown in Fig. 3(e). Finally, Fig. 3(f) presents the critical SOI as a function of the ZNR width ($Y=2|y|$), indicating a decrease in critical SOI with increasing ZNR width.

Similar to the pseudo-graphene sheet, the critical SOI for the transition from the trivial phase to the QSH phase in the ZNRs is t_{so-c}= 0.096. Despite the existence of a band gap at this intensity for various ribbon widths, the gap was more pronounced for smaller sizes. If we interpret the narrowing of the band gap as the basis for the transition to the QSH state, it becomes evident that nanoribbons with smaller sizes undergo a transition at higher spin-orbit intensity.

Table 1. The detailed exploration of how the band gap size.

t_{so}	ZNR width	15 (atoms)	30 (atoms)	60 (atoms)	100 (atoms)
			E_{gap} (eV)		
0.05		0.4834	0.5254	0.4982	0.4868
0.096		0.0594	0.0312	0.0198	0.1146

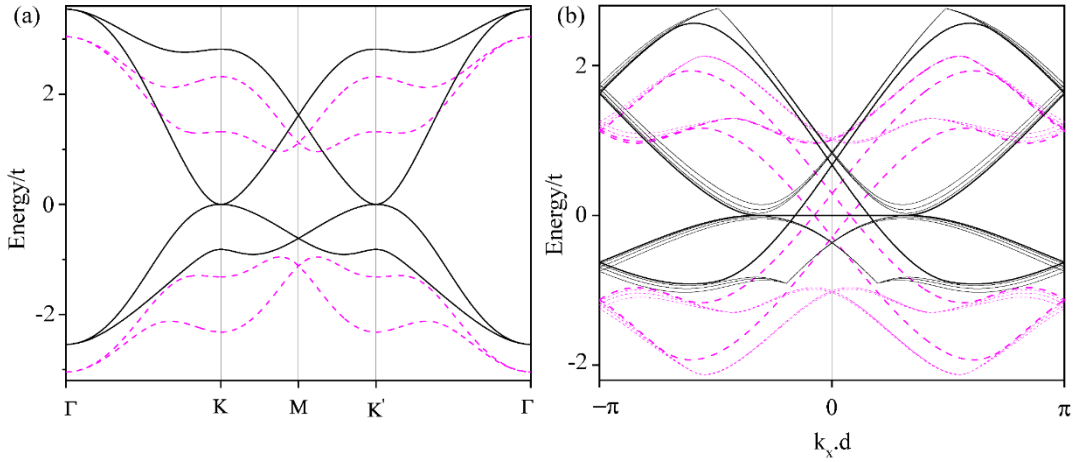

Fig. 4. Band structures of a) pseudo-graphene with the same and non-identical SOI, and band structure of b) ZNRs with the same and non-identical SOI, respectively, in purple dashed line and black solid line.

In Fig. 3(f), $t_{so\text{-}c}$ is illustrated for different nanoribbon sizes. Notably, $t_{so\text{-}c}$ decreases as the nanoribbon width increases. Nanoribbons with wider dimensions converge to t_{so}= 0.096, representing the critical spin-orbit intensity observed in the pseudo-graphene sheet.

At $t_{so} = 0$, a gap exists between the valence and conduction energy bands, which is equivalent to the energy disparity at the two-base atomic sites. This gap renders the nanoribbon completely nonmagnetic, and its size remains constant regardless of the nanoribbon width. In this context, the energy band exhibits smoothness between the K', K points, with the electron group velocity approaching zero in this energy band region. With increasing SOI, both the spin-up band gap at the K point and the spin-down band gap around the K' point decrease. The energy band structures exhibit clear time reversal symmetry.

Table 1 provides a detailed exploration of how the band gap size can be precisely adjusted by considering the number of atoms in the unit cell, providing valuable insights into both trivial and QSH phases. This analysis delves into the fascinating interplay between the structural dimensions and resulting electronic properties.

Effect of non-equal SOI for each base in a unit cell on honeycomb pseudo-graphene and ZNR

In this section, we explore the energy band structures of honeycomb pseudo-graphene and ZNRs with atoms of different types, each characterized by distinct spin-orbit intensity values for type A (t_{so}) and B (t'_{so}) atoms. Specifically, we assume that the spin-orbit intensity is zero for an atom ($t'_{so=0}$). It is imperative to provide a concise comparative analysis between this specific state and the one discussed in the previous section.

Fig. 4(a) illustrates the energy band associated with pseudo-graphene. The computations reveal that the introduction of varying spin-orbit strengths for lattice atoms disrupts the energy band symmetry relative to the Fermi surface. This perturbation leads to the closure of a band gap and the subsequent transition to the QSH phase, initiating the generation of spin current along the edges of the material.

The energy band associated with the ZNRs in a state where the Fermi energy is considered to be zero is illustrated in Fig. 4(b). As mentioned in the previous subsection, the spin-orbit intensity was the same for both atoms. If we consider the spin-orbit intensity to be zero for atom B and only atom A has a significant SOI, the symmetry of the energy

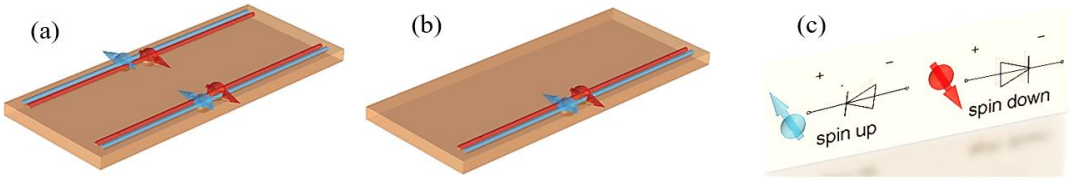

Fig. 5. Key concepts: a) existence of a rotating spin current, b) the spin current at one edge (middle state), and c) conceptualization of the spin diode.

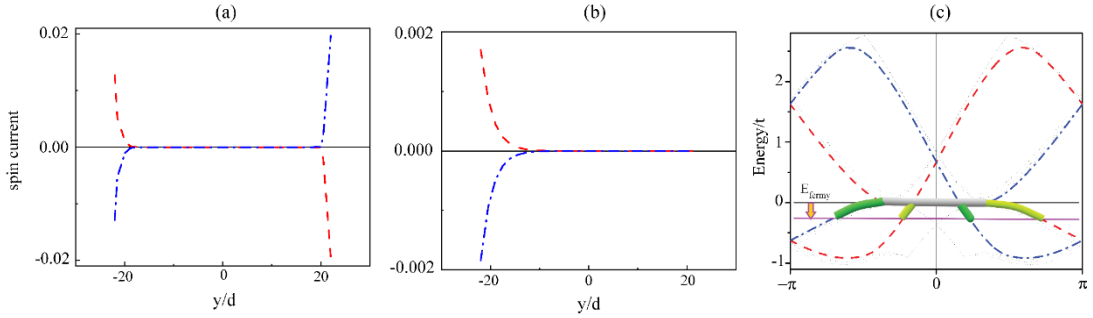

Fig. 6. spin-up and spin-down current (30 atoms in unit cell) a) on both edge, b) on one edge (middle state), and c) schematic of the band structure and the contribution of spin-up (dark green) and spin-down (pale green) carriers.

band seen earlier is disrupted. This asymmetry concerning the Fermi surface results in a different spin current, which we attempt to explain further by measuring it, thus explaining the initial idea of the spin diode.

Hence, we explain how our device responds to spin currents. We focus on adjusting parameters such as spin-orbit intensity and provide a brief overview of the structure of the device, highlighting its flexibility in adapting to parameter changes. We explore the details of the design and explain how variations in spin-orbit intensity affect device performance. We also discuss the reasons for selecting specific parameters, providing insight into the principles governing spin current. This concise exploration offers a clear understanding of the engineering of the device, its ability to respond to different spin configurations, and its potential applications in spin-current operations.

Fig. 5(a) illustrates the distribution of spin current on both edges of the two-dimensional material. The spin current is localized on one edge, referred to as the middle state, by manipulating the spin-orbit intensities at each atom in the unit cell, as shown in Fig. 5(b). This intriguing behavior has led to the conceptualization of spin diodes. The spin diode is envisioned as a device that restricts the flow of spin-up and spin-down currents to one direction exclusively because of its inherently unidirectional nature. Similar to a traditional diode that controls the flow of electrical current, the spin diode guides the flow of the spin current in one direction, as illustrated in Fig. 5(c).

Fig. 6(a) displays the spin current on both edges, establishing a connection between the rotating current and the QSH phase. Importantly, this connection remains consistent irrespective of the current's strength. Transitioning to the middle state in Fig. 6(b) results in the current being exclusively located on one side. This configuration allows us to selectively observe either a spin-up or spin-down current at the device's output. This selectivity is achieved by designing a device that facilitates current transfer in only one direction.

In our previous studies [6, 9], we conducted detailed calculations of spin currents to elucidate this perspective. However, the band structure of the middle state presents a noteworthy feature where a substantial spin current is exclusively present on one edge, introducing a unique dimension. In particular, on the Fermi surface, the velocities of the spin-up and spin-down carriers reach zero, contingent on the orbital spin intensity, as depicted by the gray shaded segment in Fig. 6(c). The manifestation of the spin current is confined to the highlighted impulses in green in Fig. 6(c).

Control of the Fermi level in the middle state is particularly intriguing. Utilizing a gate voltage, as illustrated in the figure below, allows placement

of the Fermi level in either the hole region (for negative gate voltage) or the electron region (for positive gate voltage). This precise control facilitates the manipulation of carrier types and spins, as exemplified by the spin-up and spin-down current of holes. The application of a gate voltage enables the manipulation of the Fermi level in the hole-dominant region, as depicted in Fig. 6(c). The energy band illustrates current carriers resembling spin-up and spin-down currents, which actively participate in the conduction process. However, the carriers located on the Fermi surface do not contribute to the spin current owing to their zero-group velocity.

Moreover, by applying a positive gate voltage to the electrons, similar computations and conclusions can be drawn for holes. This approach exhibits high versatility in tailoring the spin currents according to the desired output.

CONCLUSION

This extensive research delved into the vast potential of advanced electronics using two-dimensional honeycomb materials. Specifically, we investigated ZNRs and uncovered their remarkable capabilities, including the generation of zero-energy band gaps, manipulation of SOI, and facilitation of spin current. Through an in-depth exploration of the quantum spin Hall state, we demonstrated the versatility of the Kane-Mele model across various honeycomb lattices.

Our study provided intricate insights into the Hamiltonian, conducted comprehensive computational analyses of band structures, and introduced an innovative spin-filtering technique tailored specifically for ZNRs. This groundbreaking approach holds great promise for revolutionizing spintronics technology, offering a pathway to efficiently manipulate spin currents and enhance the functionality of future electronic devices. The findings of this research contribute significantly to the understanding of quantum states in honeycomb nanoribbons and can potentially drive advancements in electronic technologies based on spin.

CONFLICT OF INTEREST

The authors declare no conflicts of interest.

REFERENCES

[1] Geim A. K., Novoselov K. S., (2007), The rise of graphene. *Nature Mater*. 6: 183-191. https://doi.org/10.1038/nmat1849

[2] Tao L., (2017), Silicene field-effect transistors operating at room temperature. *Nature Nanotechnol.* 10: 227-231. https://doi.org/10.1038/nnano.2014.325

[3] Dávila M. E., (2014), Germanene: A novel two-dimensional germanium allotrope akin to graphene and silicene. *New J. Phys.* 16: 095002. https://doi.org/10.1088/1367-2630/16/9/095002

[4] Tao C., (2011), Spatially resolving edge states of chiral graphene nanoribbons. *Nature Phys.* 7: 616-620. https://doi.org/10.1038/nphys1991

[5] Yazyev O. V., (2010), Emergence of magnetism in graphene materials and nanostructures. *Rep. on Prog. Phys.* 73: 056501. https://doi.org/10.1088/0034-4885/73/5/056501

[6] Ghorbani J., (2023), Magnetic edge states and edge current in honeycomb zigzag nanoribbons by Kane–Mele–Hubbard model. *Solid State Communic.* 371: 115250. https://doi.org/10.1016/j.ssc.2023.115250

[7] Enoki T., (2012), Zigzag and armchair edges in graphene. *Carbon*. 50: 3141-3145. https://doi.org/10.1016/j.carbon.2011.10.004

[8] Ezawa M., Nagaosa N., (2013), Interference of topologically protected edge states in silicene nanoribbons. *Phys. Rev. B*. 88: 121401(R). https://doi.org/10.1103/PhysRevB.88.121401

[9] Baradaran A., Ghaffarian M., (2020), Bias-voltage-induced topological phase transition in finite size quantum spin Hall systems in the presence of a transverse electric field. *Phys. E: Low-dimens.l Sys. Nanostruc.* 122: 114173-114177. https://doi.org/10.1016/j.physe.2020.114173

[10] Brey L., Fertig H. A., (2006), Electronic states of graphene nanoribbons studied with the dirac equation. *Phys. Rev. B*. 73: 235411-235416. https://doi.org/10.1103/PhysRevB.73.235411

[11] Kane C. L., Mele E. J., (2005), Quantum spin hall effect in Graphene. *Phys. Rev. Lett.* 95: 226801-226805. https://doi.org/10.1103/PhysRevLett.95.226801

[12] Kane C. L., Mele E. J., (2005). Z2 topological order and the quantum spin hall effect. *Phys. Rev. Lett.* 95: 146802-146810. https://doi.org/10.1103/PhysRevLett.95.146802

[13] Haldane F. D. M., (1988), Model for a Quantum Hall Effect without Landau Levels: Condensed-Matter Realization of the "Parity Anomaly". *Phys. Rev. Lett.* 61: 2015-2021. https://doi.org/10.1103/PhysRevLett.61.2015

[14] Hasan M. Z., Kane C. L., (2010), Colloquium: Topological insulators. *Rev. Modern Phys.* 82: 3045-3052. https://doi.org/10.1103/RevModPhys.82.3045

[15] Ezawa M., (2012), A topological insulator and helical zero mode in silicene under an inhomogeneous electric field. *New J. Phys.* 14: 033003. https://doi.org/10.1088/1367-2630/14/3/033003

[16] Cahangirov S., (2009), Two- and one-dimensional honeycomb structures of silicon and germanium. *Phys. Rev. Lett.* 102: 236804-236814. https://doi.org/10.1103/PhysRevLett.102.236804

[17] Xu, Y., (2013), Large-gap quantum spin Hall insulators in tin films. *Phys. Rev. Lett.* 111: 136804-136813. https://doi.org/10.1103/PhysRevLett.111.136804

[18] Shitade A., (2009), Quantum spin hall effect in a transition metal oxide Na_2IrO_3. *Phys. Rev. Lett.* 102: 256403-256414. https://doi.org/10.1103/PhysRevLett.102.256403

[19] Wang Z. F., (2013), Organic topological insulators in organometallic lattices. *Nature Communic.* 4: 1471-1477.

https://doi.org/10.1038/ncomms2451
[20] Avsar A., (2017), Spin–orbit proximity effect in graphene. *Nature Communic.* 8: 702-709. https://doi.org/ 10.1038/ncomms5875
[21] Han W., (2014), Graphene spintronics. *Nature Nanotechnol.* 9: 794-807. https://doi.org/10.1038/nnano.2014.214
[22] Sadjadi M. S., Sadeghi B., Zare K., (2007), Natural bond orbital (NBO) population analysis of cyclic thionylphosphazenes, [NSOX $(NPCl_2)_2$]; X = F (1), X = Cl (2). *J. Molec. Struc: THEOCHEM*. 817: 27-33. https://doi.org/10.1016/j.theochem.2007.04.015
[23] Dadashi H., Hajinasiri R., (2020), Biosynthesis of Cu and CuO nanoparticles using aqueous leaves extract of Sambucus nigra L. *Int. J. Nano Dimens.* 11: 405-411. 20.1001.1.20088868.2020.11.4.10.4
[24] Abdel Halim S., (2018), Electronic structures and stabilities of endohedral metallofullerenes TM@C34 using DFT approach. *Int. J. Nano Dimens.* 9: 421-434. 20.1001.1.20088868.2018.9.4.9.9
[25] Esfahani S., (2023), Assessing the drug delivery of ibuprofen by the assistance of metal-doped graphenes: Insights from density functional theory. *Diamond and Related Mater.* 135: 109893-109898. 10.1016/j.diamond.2023.109893
[26] Saadh M. J., (2024), Density functional theory assessments of an iron-doped graphene platform towards the hydrea anticancer drug delivery. *Diamond and Related Mater.* 141: 110683-110686. 10.1016/j.diamond.2023.110683
[27] Pecho R. D. C., (2023), Molecular insights into the sensing function of an oxidized graphene flake for the adsorption of Avigan antiviral drug. *Comput. Theoret. Chem.* 1227: 114240-114246. 10.1016/j.comptc.2023.114240
[28] Saadh M. J., (2023), An enhanced adsorption of paracetamol drug using the iron-encapsulated boron carbide nanocage: DFT outlook. *Comput. Theoret. Chem.* 1227: 114421-114427. 10.1016/j.comptc.2023.114421